

COMPUTATION OF CAPILLARY SURFACES FOR THE LAPLACE-YOUNG EQUATION

by C. F. SCOTT, G. C. SANDER

(Department of Civil & Building Engineering, Loughborough University,
Loughborough, LE11 3TU, UK.
email: c.f.scott@lboro.ac.uk, g.sander@lboro.ac.uk)

and J. NORBURY

(The Mathematical Institute, Oxford University,
24-29 St Giles, OX1 3LB, UK.
email: norbury@maths.ox.ac.uk)

[Received 20 February 2004. Revise 24 May 2004]

Summary

A novel hybrid finite-element/finite-volume numerical method is developed to determine the capillary rise of a liquid with a free surface (under surface tension and gravitational forces). The few known exact analytical solutions are used to verify the numerical computations and establish their accuracy for a range of liquid contact angles. The numerical method is then used to ascertain the limitations of a number of theoretical approximations to solutions for the capillary rise in the linearized limit, for special geometries such as plane walls, concentric cylinders and in a wedge of arbitrary included angle. The existence of a critical wedge angle for a given contact angle is verified. However, the effect of slight practical rounding of wedge corners dramatically reduces the theoretical corner height.

1. Introduction

Industrial processes involve dipping objects such as semiconductor devices and spectacle lenses into stationary liquids, and the wetted surface edge often determines the success of the process. Fowkes and Hood (1) comment on the lack of exact solutions and the need for numerical solutions especially in the non-linear regime. We suggest a new numerical approach to solving the traditional Laplace-Young equation with non-linear contact condition, that describes how the liquid surface $\tilde{u}(\tilde{x}, \tilde{y})$ wets the vertical sidewalls.

It is known that corner effects may dominate the shape of the air-liquid interface near the boundary of the dipped object. Also, as is well known, sufficiently high curvatures (and associated forces) of pipes micrometers in diameter in plants and trees enable liquids to rise to heights of tens of meters against gravity; curvature forces even allow for liquid to collect in lung passageways and block breathing. The reason for this marked behaviour is also the major cause of difficulty in the numerical solution of the capillary surface rise problem, that is, the non-linear dependence of the flux function $\tilde{\mathbf{F}}(\tilde{u})$ defined by

$$\tilde{\mathbf{F}}(\tilde{u}) = \frac{-\nabla \tilde{u}}{\sqrt{1 + \nabla \tilde{u} \cdot \nabla \tilde{u}}} = -K(\nabla \tilde{u}) \nabla \tilde{u} \quad (1.1)$$

on the surface $\tilde{u}(\tilde{x}, \tilde{y})$.

We consider the equilibrium of such a surface $\tilde{z} = \tilde{u}(\tilde{x}, \tilde{y})$, the surface forming the upper boundary of the static fluid lying in a container with horizontal flat base A and vertical sidewalls. With \tilde{z} measuring distance upwards from the base, the gravitational force in the static bulk of the fluid is given by $\rho g \tilde{u}$, where ρ is the density of the fluid and g is the acceleration due to gravity. The pressure on the upper surface $\tilde{z} = \tilde{u}(\tilde{x}, \tilde{y})$ is due to the air above, and is taken as the constant p_0 . The only other forces we consider are the surface tension $\sigma \nabla \cdot \tilde{\mathbf{F}}(\tilde{u})$, which is the liquid surface tension constant σ times the curvature of the surface, and the contact forces where the surface meets the sidewalls above the boundary ∂A of the base.

Our force balance, or equilibrium, equation is now written at a point $(\tilde{x}, \tilde{y}) \in A$ and $\tilde{z} = \tilde{u}(\tilde{x}, \tilde{y})$ as

$$\nabla \cdot \tilde{\mathbf{F}} = - \left(\frac{\rho g}{\sigma} \right) \tilde{u} \quad (\tilde{x}, \tilde{y}) \in A, \quad (1.2)$$

where we have measured $\tilde{z} = \tilde{u}(\tilde{x}, \tilde{y})$ from the origin so that the constant atmospheric pressure p_0 is taken into the gravitational head pressure. This change of height origin does not affect the surface curvature or contact angle terms. The surface tension force of the liquid is modified where the liquid touches the sidewalls and this is known as the contact condition, which is usually written as

$$\tilde{\mathbf{F}} \cdot \mathbf{n} = -\cos \gamma \quad (\tilde{x}, \tilde{y}) \in \partial A, \quad (1.3)$$

which holds on the boundary ∂A of domain A . Here, \mathbf{n} is the unit outward normal at the boundary and γ is the contact angle and measures the strength of adhesion of the liquid surface to the solid boundary, normalized so that $\gamma = \pi/2$ represents zero contact force and $\gamma = 0$ gives the maximum. The usual derivation of these equations (see Finn, **2**) follows from an energy functional which includes surface energy and gravitational potential energy; equation (1.3) then arises as a natural boundary condition for the problem given in equation (1.2).

We interpret this problem as supplying \tilde{u} at the constant rate $\cos \gamma$ at the boundary (a source), while losing \tilde{u} at a rate $(\rho g / \sigma) \tilde{u}$ in the interior of A (a sink), with the non-linear flux $\tilde{\mathbf{F}}$ diffusing \tilde{u} down $\nabla \tilde{u}$ with non-linear diffusivity $K(\nabla \tilde{u})$. For small $|\nabla \tilde{u}|$, we have a conventional linear elliptic Helmholtz partial differential equation with a Neumann boundary condition, whereas for large $|\nabla \tilde{u}|$ we have a singular limit partial differential equation with unusual solution behaviour (see King *et al.*, **3**). Very few explicit solutions of this problem are known (see §3 for descriptions of these) and we wish to find an effective computational procedure.

We use an unstructured triangulation of the domain A and linear representations of \tilde{u} on the triangular volumes from which we can then numerically represent \tilde{u} and $\nabla \tilde{u}$ exactly on each triangle. By matching these representations across the triangular boundaries using the divergence theorem on each triangle to conserve the “mass” of the density $\tilde{u}(\tilde{x}, \tilde{y})$, equation (1.2) is converted into a relation between the loss of \tilde{u} on each volume element to the flux of \tilde{u} across the element boundaries. The accuracy of our numerical method is verified on several levels in both one and two dimensions. Checks are performed against (i) the exact one-dimensional plane wall solutions for both finite and semi-infinite domains (Landau and Lifshitz, **4**), (ii) the linearized analytical solutions of Fowkes and Hood (**1**)

applying in semi-infinite wedges, (iii) numerical solutions of the full non-linear ordinary differential equation for describing the radially symmetric surface occurring between two concentric cylinders and (iv) the regular power series expansion about the wedge corner at $r = 0$ to any order in r , of the full non-linear equation for $\tilde{u}(\tilde{r}, \theta)$ developed by Norbury *et al.* (5). We find that once $\gamma < 80^\circ$ ($\cos \gamma > 0.2$), non-linearity is important in practice and that even a little rounding of corners has a dramatic effect on reducing the liquid rise in the corner. The original reason for the industrial problem described by Fowkes and Hood (1), was to understand the arching effect of the wetted boundary at an exterior corner of a dipped object (known as mooning), and we comment on this as well.

What appears in these various solutions is the importance of both the capillary length scale $(\sigma/\rho g)^{1/2}$ and the local length scale arising from boundary curvature. Our unstructured grid allows us to focus elements where the variation is strongest, whereas our hybrid triangle-finite-volume approach allows us to exactly and consistently approximate all terms in the partial differential equation and boundary conditions with linear basis functions. We are thus left with a large non-linear but sparse matrix inversion, which appears to be robust and stable and can be handled by various existing methods with differing degrees of sophistication.

We non-dimensionalize lengths by the capillary length scale $d = (\sigma/\rho g)^{1/2}$, so that $\tilde{x} = dx$, $\tilde{y} = dy$ and scale $\tilde{u}(x, y)$ by the same factor d . Our rescaled problem becomes

$$\nabla \cdot (-K(\nabla u) \nabla u) = -u \quad (x, y) \in A, \quad (1.4)$$

$$-K(\nabla u) \nabla u \cdot \mathbf{n} = -\cos \gamma \quad (x, y) \in \partial A. \quad (1.5)$$

The linearized (small $\cos \gamma$) version of this problem is $\nabla \cdot (\nabla u) = u$ in A and $\nabla u \cdot \mathbf{n} = \cos \gamma$ on ∂A , where (using the divergence theorem) $\int_A u dx dy = \int_{\partial A} \cos \gamma ds$. Thus the net volume of lifted fluid over A is equal to the total lifting force at the boundary ∂A for this linearized problem. We check that our calculations respect the corresponding identity for the non-linear problem of equations (1.4-1.5). We also note that this linearized elliptic problem is uniquely solvable with the boundary conditions in bounded domains A with smooth boundaries on which equation (1.5) holds, or mixed Dirichlet contact or homogeneous Neumann boundary conditions, etc. However, the non-linear problem may have more solution possibilities when the geometry of A is more complex. For instance, we see later that a corner with a narrow angle implies that $u \rightarrow \infty$.

2. The Numerical Scheme

We now describe in detail the numerical method. The numerical scheme is a control-volume-based finite-element approach with an unstructured triangular vertex-centred mesh as used by Baliga and Pantankar (6) and described in Ferziger and Peric (7, §8.7). The solution domain A is subdivided into triangular elements and dependent variables ϕ_i are then specified at each computational node i located at the element vertices. The dependent variable ϕ is assumed to vary linearly within the element j , that is, its shape function is $\phi_j(x, y) = a_j x + b_j y + c_j$ where j ranges through the element list and the coefficients a_j , b_j and c_j are determined by fitting the function ϕ to nodal values ϕ_i at the vertices. Thus, a_j , b_j and c_j are functions of node coordinates and variable values at the nodes chosen. Note that ϕ is then continuous in the solution domain.

The control volumes are formed around each node by joining the centroids of the

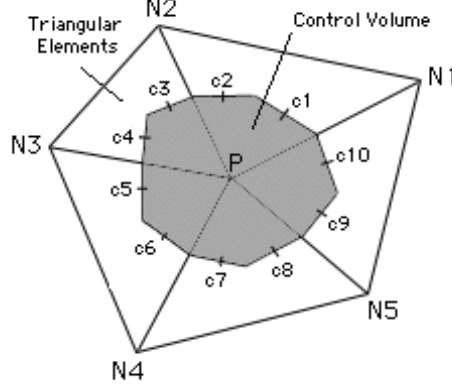


Fig. 1 Schematic of five triangular elements with common vertex P , and the control volume centred on this node P . Here, the control surface $c1$ - $c10$ is formed by joining the five triangle centroids with the five midpoints of the triangle edges meeting at P .

triangular elements to the midpoints on element edges, as shown in Figure 1 for five triangles meeting at the vertex P . In this example, the control surface on the control volume (shown coloured in grey) consists of 10 sub-surfaces and its volume consists of five sub-volumes, one in each triangle. Since the variation of variables over an element is prescribed in the form of an explicit analytic -indeed, linear - function, all integrals over such volumes can be evaluated easily.

The governing equations (1.4-1.5) are converted to a control-volume formulation by integrating over each polygonal elemental control volume and applying the divergence theorem to the left-hand-side:

$$\oint_{\partial\Delta} K(\nabla u) \nabla u \cdot \mathbf{n} \, dS = \int_{\Delta} u \, dA \quad (2.1)$$

where Δ and $\partial\Delta$ represent the polygonal element area and boundary, respectively. When the flux and density are continuous across elements, equation (2.1) represents mass conservation on each polygon of the density u which has a volume sink proportional to $K(\nabla u) \nabla u \cdot \mathbf{n}$. Here, in terms of our linear representations $u_j = a_j x + b_j y + c_j$, both sides of equation (2.1) can be evaluated exactly and efficiently. By summing these equations over all polygons in A , we go from this exact local conservation to an exact global conservation. The sum of the right-hand-side volume integrations is the exact total volume under the surface $z = u(x, y)$ above the area A enclosed by the vertical sidewalls at ∂A . Therefore, we have an identity relating the volume of fluid to the integral of the contact angle term $\cos \gamma$ around the boundary, so that $\cos \gamma \times \text{boundary length} = \cos \gamma |\partial A| = \text{volume of lifted liquid}$. Consequently, the gravitational weight of the net lifted liquid is balanced by the total tensile or contact force of the boundary on the liquid wetted edge. Of course, the remaining liquid's weight, together with the atmospheric pressure force on the surface $z = u(x, y)$ is balanced by the normal upwards force on the bottom of the container.

The equation may be simply linearized by using a diffusion coefficient $K(\nabla u)$ evaluated from gradients at the previous iteration. A more effective iteration scheme arises from Newton iteration of this contact boundary condition. A linear system of equations generated by equation (2.1) for each element with a constant flux $K(\nabla u)\nabla u \cdot \mathbf{n} = \cos \gamma$ specified at the boundary of the computational domain A , is assembled into a sparse matrix and solved using LU factorization. This process is iterated until convergence. The code is written in object-oriented Java, and uses a Java implementation of the LU factorization method for sparse matrices available from the public domain numerical package LAPACK.

3. Comparison of Numerical and Theoretical Results

We first check our numerical method by computing approximations to known (or approximately known) special geometries, those of parallel plane walls and of wedges and cylinders.

3.1 The Plane Wall Case

There are only two known exact analytic solutions to the Laplace-Young equations governing a free-surface subject to capillary action. These are for a plane vertical wall in a semi-infinite domain, and for two parallel vertical walls containing liquid between the walls. The exact solution for the single plane wall case (Landau and Lifshitz, **4**, p325 or Batchelor, **8**, p67) is given in implicit form by

$$x = \cosh^{-1} \frac{2}{u} - \cosh^{-1} \frac{2}{h} + (4 - h^2)^{1/2} - (4 - u^2)^{1/2} \quad (3.1)$$

where x is the distance from the wall, and where h , the height of the liquid surface at the wall, is given by $h^2 = 2(1 - \sin \gamma)$.

For the single plane wall case, integration of the flux balance equation (1.2) over the entire one-dimensional domain yields $\int_0^\infty u dx = \cos \gamma$, a condition also satisfied by equation (3.1). Thus, the flux lost in the interior $0 < x < \infty$ matches the flux $\cos \gamma$ entering at the boundary. This equal distribution of ‘sources’ and ‘sinks’ for the plane wall case may be illustrated by referring to Figure 2. The source at the boundary wall is of fixed strength $\cos \gamma$ while the strength of the each sink is proportional to the surface elevation, u . Since the largest sink is nearest the boundary source, changes in elevation are confined to a distance of the order of the capillary length scale d from the boundary.

The computational domain for our 2-D numerical method was chosen as a strip one capillary length scale d wide and $10d$ long. Table 1 shows the results for numerical computation for the plane wall case for varying contact angles applied to a short wall and zero contact angles (hence, zero flux) applied on the remaining. Increasing the length of the strip beyond $10d$ had no effect on the accuracy shown in the table. Initially an approximate triangular mesh was generated with a mesh density roughly proportional to the slope of the free surface. The solution was then computed, the mesh regenerated to better satisfy the same requirement and the solution recomputed. The final mesh consisted of about 18,000 elements.

The results in Table 1 show that the computed free surface height at the wall is reasonably accurate. For instance, the relative error in wall height for the severe case of a 1 degree

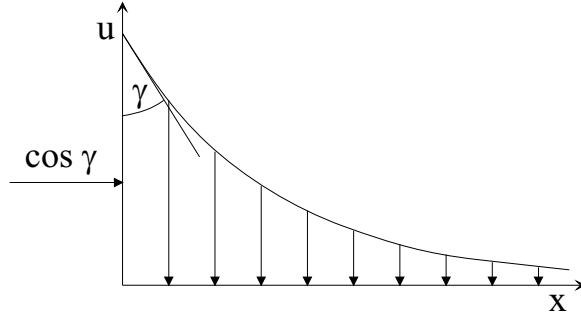


Fig. 2 The distribution of ‘sources’ of strength $\cos \gamma$ at the boundary (here, $x = 0$) and ‘sinks’ of strength u in the interior ($x > 0$) for a capillary surface near a plane wall.

| Contact Angle (degrees) | Theoretical Height | Computed Height | Computed Height Relative Error |
|-------------------------|--------------------|-----------------|--------------------------------|
| 1 | 1.4018 | 1.3777 | 1.72×10^{-2} |
| 5 | 1.3512 | 1.3459 | 3.91×10^{-3} |
| 10 | 1.2856 | 1.2840 | 6.86×10^{-4} |
| 30 | 1.0000 | 0.9993 | 6.86×10^{-4} |
| 45 | 0.7654 | 0.7648 | 6.79×10^{-4} |
| 60 | 0.5176 | 0.5173 | 6.82×10^{-4} |
| 75 | 0.2611 | 0.2609 | 6.82×10^{-4} |

Table 1 Numerical results for a plane wall for various angles of contact.

contact angle is less than 2%. Figure 3 shows the scatter-plot of computed nodal elevations versus distance from the wall superimposed on the theoretical plane wall solution given by equation (3.1) to be in close agreement. On a larger scale, there was no significant difference between the two quantities. However, on a finer scale near the wall, differences arise from an inability to resolve the surface slope. Inspection of the curvature of the theoretical solution in Figure 3 shows that, for a 5 degree contact angle, length scales of the order of at least 10^{-3} need to be resolved for extreme accuracy. For a 1 degree contact angle, length scales of the order of 3×10^{-4} need to be resolved. Even if the graphically-based grid generator that was used to generate the mesh were able to achieve this, one would be faced with a massive increase in computational cost. These results serve to indicate some of the strengths and limitations of the numerical scheme. However, exact flux conservation means that global accuracy can be maintained even if some very local near-wall accuracy is lost.

3.2 The Wedge

There have been a number of approximate analytical results derived (by using asymptotic expansions) for the elevation of the free surface of a liquid with a specified contact angle confined to a wedge-shaped region. Figure 4 shows the variables and wedge geometry used in this discussion. For plane polar coordinates (r, θ) centred on the apex of the wedge, we

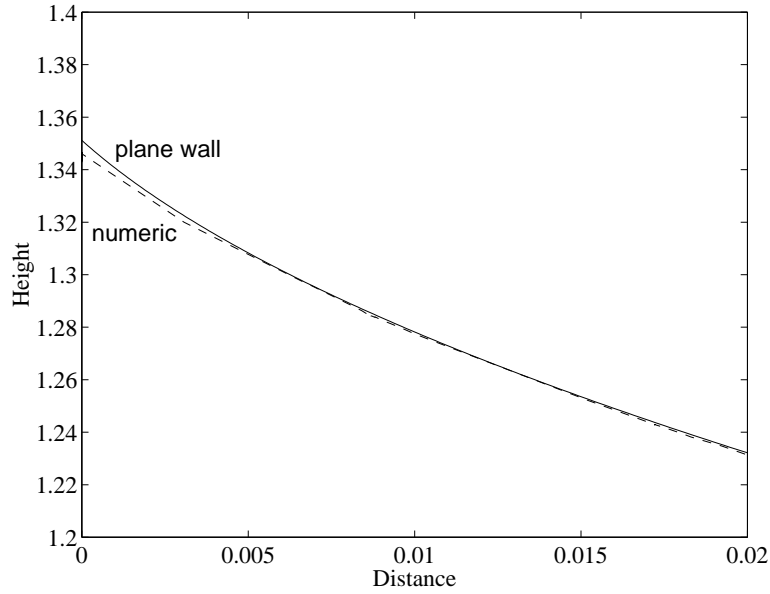


Fig. 3 Near-wall behaviour for a 5 degree contact angle, showing numerical error very near the wall of about 1%.

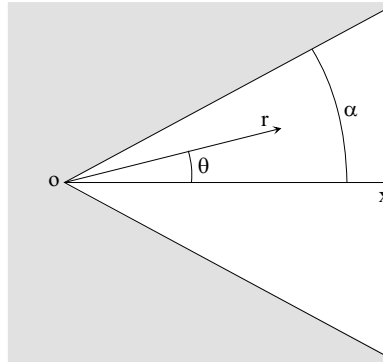


Fig. 4 The wedge geometry - α is the wedge half angle and the wedge is semi-infinite in the region $0 \leq r < \infty$, $|\theta| \leq \alpha$.

have a symmetric liquid plan of $0 < r < \infty$, $|\theta| \leq \alpha$, together with vertical sidewalls at $\theta = \pm\alpha$. Numerical computations, however, were naturally restricted to a finite domain $0 < r < R$, $|\theta| \leq \alpha$ with the contact angle (i.e., flux) specified at $\theta = \pm\alpha$, and set to zero on the radial boundary at $r = R$. R was reduced in stages from a sufficiently large value until the corner height just began to be affected to 5 decimal places. This fixed the radial boundary at $R = 10$ for the simulations.

Linearized Solutions

For contact angles close to $\pi/2$, we have ∇u being small over all the liquid surface, the flux simplifies as $\nabla u / \sqrt{1 + |\nabla u|^2} \approx \nabla u$ and equation (1.2) reduces to $\nabla^2 u = u$. Hence, the governing equation is asymptotically linear. Near the corner of a wedge with half-angle α , the solution represented by the first two terms of the asymptotic expansion is given by (Fowkes and Hood, **1**)

$$u(r, \theta) = \cos \gamma \left(\frac{\pi}{2\alpha} - \frac{r \cos \theta}{\sin \alpha} \right) + O(r^2). \quad (3.2)$$

Design engineers are usually concerned with the wetted boundary, that is, $u(r, \alpha)$ for $\theta = \alpha$ in the case of a wedge. At large distances from the corner, the linearised plane wall solution of Fowkes and Hood (**1**) is given by $\cos \gamma$. Hence, from equation (3.2), it follows that the linear extent of arching from the corner is $\cos \gamma(1 - \pi/2\alpha)$. For the non-linear equations, the extent of arching is given by $h - u_0$, where u_0 is the numerically calculated corner height and h is the plane wall height from equation (3.1). Table 2 shows the results of numerical

| Contact Angle (degrees) | Computed Wall Height | Computed Extent of Arching | Linearized Arching | Relative Error |
|-------------------------|----------------------|----------------------------|--------------------|----------------|
| 1 | 1.3777 | 0.6107 | 0.3333 | 0.4542 |
| 5 | 1.3459 | 0.5831 | 0.3321 | 0.4306 |
| 10 | 1.2840 | 0.5342 | 0.3283 | 0.3855 |
| 30 | 0.9993 | 0.3689 | 0.2887 | 0.2176 |
| 45 | 0.7648 | 0.2687 | 0.2357 | 0.1229 |
| 60 | 0.5173 | 0.1764 | 0.1667 | 0.0553 |
| 75 | 0.2609 | 0.0876 | 0.0863 | 0.0146 |

Table 2 Comparison of computed and linearized (first order) extent of arching for a wedge half-angle of $3\pi/4$, showing that the linear approximation is only useful for contact angles $\gamma < \pi/4$.

computation for a right-angled wedge ($\alpha = 3\pi/4$) and shows the computed extent of arching versus the linear approximation. The mesh consisted of approximately 10,000 elements. Our confidence in the numerical solutions obtained for both the plane wall and corner series expansion (see next section) cases suggests that the same level of accuracy for wall and corner height computations applies here. This leads us to conclude that for an accuracy of 2% or better, the linear solution is really limited to contact angles of 75 degrees or more. This is not unexpected since the asymptotic expansion was derived for the shallow contact angle limit. The useful consequence of these results is that we are now able to quantitatively define the region of applicability of the linearized Fowkes and Hood (**1**) solution.

Non-Linear Solutions

Norbury *et al.* (**5**) derive a regular series expansion of the form

$$u(r, \theta) = u_0 + ru_1(\theta) + r^2u_2(\theta) + r^3u_3(\theta) + \dots = \sum_{n=0}^{\infty} r^n u_n(\theta) \quad (3.3)$$

valid only for r small and for intermediate corner angles $\pi/2 - \gamma < \alpha < \pi/2$ where the far field has negligible influence on the corner behaviour. While all $u_n(\theta)$, $n = 2, 3, \dots, \infty$ are known explicitly, u_n for $n \geq 2$ require u_0 which can only be found numerically. The accuracy of the numerical solution can then be verified by using the numerically calculated u_0 in equation (3.4) and seeing how well the series matches the computed results away from $r = 0$. Figure 5 demonstrates the excellent match between the two obtained along the wall $\theta = \alpha = \pi/6$ for a contact angle $\gamma = \pi/4$. As the order of the expansion is increased, better agreement with the numerically computed solution is found over greater r , consistently.

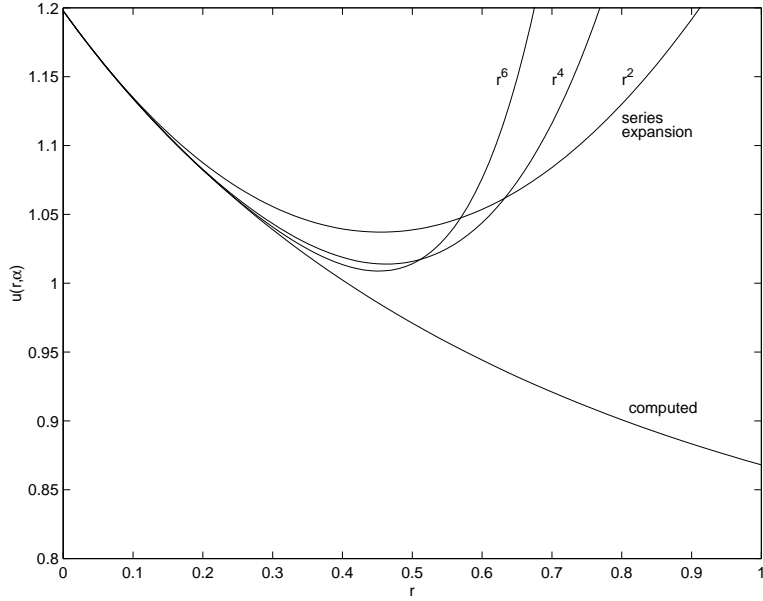


Fig. 5 Comparison of regular power series and the numerical solution on $\theta = \alpha$ near the corner for $R = 6$ with $\alpha = \pi/6$ and $\gamma = \pi/4$.

Singular Corner Behaviour

For sufficiently small wedge angles $\alpha < \pi/2 - \gamma$, solutions are known to be unbounded at the corner and given by (Concus and Finn, **9**, **10**)

$$u = \frac{\cos \theta - \sqrt{k^2 - \sin^2 \theta}}{kr} + \mathcal{O}(r^3) \quad (3.4)$$

where $k = \sin \alpha / \cos \gamma$. Table 3 shows that for a wedge angle $\alpha = \pi/4$, our numerical computations reveal that the corner heights indeed approach infinity as γ tends to the critical contact angle $\pi/4$.

In reality, corners are never perfect and there is always some degree of rounding. For comparison, we have included in Table 2.1 the results for numerical computations for wedges with rounded corners with the radius non-dimensionalized by the capillary length scale.

| Contact Angle (degrees) | $R_c = 0$ | $R_c = 0.10$ | $R_c = 0.25$ | $R_c = 0.5$ | $R_c = 1$ |
|-------------------------|-----------|--------------|--------------|-------------|-----------|
| 85 | 0.3655 | 0.2694 | 0.2199 | 0.1788 | 0.1429 |
| 80 | 0.7509 | 0.5409 | 0.4397 | 0.3572 | 0.2854 |
| 75 | 1.606 | 0.8155 | 0.6597 | 0.5348 | 0.4278 |
| 70 | 29.43 | 1.096 | 0.8796 | 0.7112 | 0.5672 |
| 65 | 56.42 | 1.384 | 1.100 | 0.8859 | 0.7056 |
| 60 | 82.06 | 1.688 | 1.321 | 1.060 | 0.8437 |
| 45 | ∞ | 2.798 | 1.989 | 1.562 | 1.236 |
| 30 | ∞ | 4.732 | 2.684 | 2.031 | 1.593 |
| 10 | ∞ | 8.078 | 3.648 | 2.549 | 1.971 |
| 5 | ∞ | 8.756 | 3.833 | 2.614 | 2.025 |
| 1 | ∞ | 9.009 | 3.904 | 2.650 | 2.043 |

Table 3 Computed corner heights for varying contact angles for a rounded corner of dimensionless radius R_c for an $\alpha = \pi/8$ wedge, showing the dramatic effect of small corner rounding on controlling (singular) capillary height rise.

Although a more thorough mathematical and numerical analysis will be left to a subsequent paper, these computations already show that the effect of corner rounding is dramatic in terms of controlling the capillary height rise.

3.3 Concentric Cylinders

To further demonstrate the accuracy of the numerical method, the full 2-D numerical solution was compared with solution for the equivalent radial 1-D axis-symmetric problem. As there is no known analytical solution for the radial 1-D problem, the governing equation

$$-F_r = \left[\frac{ru}{(1 + u_r^2)^{1/2}} \right]_r = ru \quad (3.5)$$

was solved by the finite volume method with the flux F specified as $F = R_0 \cos \gamma$ and $F = -R_1 \cos \gamma$ at the cylinder boundaries at $r = R_0$ and $r = R_1$, respectively. For the 2-D problem, a uniform mesh comprising some 13,000 triangular elements was constructed over the same domain bounded by $R_0 = 1$ and $R_1 = 10$, and a similar resolution was used for the radial 1-D equivalent. Figure 6 shows the comparison for a $\pi/4$ contact angle on both cylinders. The 2-D results are given as a scatter plot of nodal elevations versus radial distance from the origin. Figure 6 is presented in this form since the unstructured mesh does not *a priori* position nodal points along a radial line. Again, we have good agreement over the solution domain.

4. Summary

A hybrid finite-element/finite-volume numerical method has been developed to compute the capillary rise against gravity for a static liquid contained by vertical sidewalls. Using an unstructured triangular mesh, our method is able to compute the meniscus height in

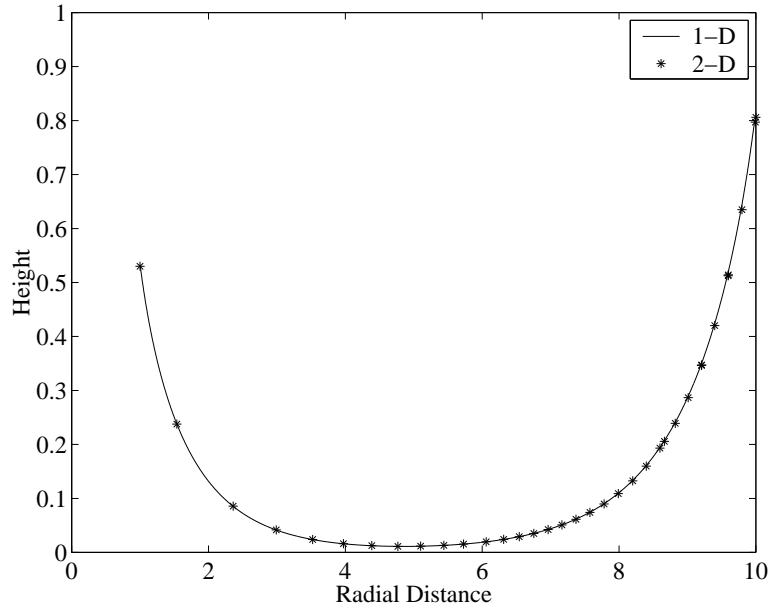


Fig. 6 Comparison of numerical non-dimensionalized solutions for the meniscus height between two concentric cylinders of radius $r = 1$ and $r = 10$ of a fluid with contact angle $\pi/4$ using the full 2-D solver and the axially-symmetric 1-D problem.

arbitrarily shaped domains. A formulation in terms of an iterated, but specified linear boundary flux, instead of a wall contact angle, leads to results that converge to the correct contact angle at the wall. The method is second-order accurate, robust and stable and has been validated using known theoretical results, both exact analytic and asymptotic. The method is used on various test problems to show its use in practical applications, for instance, the slight rounding of theoretically sharp corners in practice (see Table 3), showing the dramatic effect of such small practical effects on the theoretical results for perfect corners.

References

1. Fowkes, N. D. and M. J. Hood. Surface tension effects near a wedge. *Q. Jl Mech. Appl. Math.*, **51**(4) (1998), 553-561.
2. Finn, R. *Equilibrium Capillary Surfaces*. Springer-Verlag, Berlin-Heidelberg-New York (1986).
3. King, A. C., J. R. Ockendon and H. Ockendon. The Laplace-Young equation near a corner. *Q. Jl Mech. Appl. Math.*, **52**(1) (1999), 73-97.
4. Landau, L. D. and E. M. Lifshitz *Fluid Mechanics*, Course in Theoretical Physics, Volume **6**. Pergamon Press (1959).
5. Norbury, J., G. C. Sander and C. F. Scott. Corner solutions of the Laplace-Young equation. *Q. Jl Mech. Appl. Math.* (to appear).

6. Baliga, R. B. and S. V. Patankar. A control-volume finite element method for two-dimensional flow and heat transfer. *Numer. Heat Transfer*, **6** (1983), 245-261.
7. Ferziger J. H. and M. Peric. *Computational Methods for Fluid Dynamics*. Springer (1996).
8. Batchelor, G. K. *An Introduction to Fluid Mechanics*. Cambridge University Press (1967).
9. Concus, P. and R. Finn. On a class of capillary surfaces. *J. Analyse Math.*, **23** (1970), 65-70.
10. Concus, P. and R. Finn. Capillary wedges revisited. *SIAM Jl Math. Anal.*, **27**(1) (1996), 56-69.